Experimental Thermal and Fluid Science 33 (2009) 620–629

Contents lists available at ScienceDirect

Experimental Thermal and Fluid Science

journal homepage: www.elsevier.com/locate/etfs

Characterization of incipient cavitation in axial valve by hydrophone and visualization

Aljaž Osterman *, Marko Hočevar, Brane Širok, Matevž Dular

Faculty of Mechanical Engineering, University of Ljubljana, Aškerčeva 6, SI-1000 Ljubljana, Slovenia

ARTICLE INFO

Article history:
Received 20 May 2008
Received in revised form 26 September 2008
Accepted 21 December 2008

Keywords:
Incipient cavitation
Valve
Hydrophone
Visualization
Frequency spectrum

ABSTRACT

As the effects of cavitation in valves are devastating, the choice of the correct valve for a given operating range is crucial. For this, the valve characteristic is needed, whereby one side of the operating range depends on the determination of the incipient cavitation.

In this paper, the visualization method for incipient cavitation detection is presented. For the purpose of comparison, pressure oscillations inside the pipeline were simultaneously measured with a hydrophone. The effect of operating pressure was studied for two different openings of the valve.

For each operating point of incipient cavitation, corresponding points were measured for developed cavitation and no-cavitation state, based on a constant-portion change of volumetric flow rate with regard to the incipient cavitation volumetric flow rate. The visualization and hydrophone signals were compared.

The visualization method proved efficiency over hydrophone measurements because it is more sensitive to cavitation and the signal is independent of the operating pressure. The main drawback is the preparation of the observation window.

1. Introduction

Cavitation is a phenomenon that occurs in fluids, basically because local absolute pressure drops below the vapour pressure of a liquid. More harmful than vaporization is the collapse of vapour structures in regions where local absolute pressure increases back above the liquid vapour pressure.

In a valve, the flow is obstructed, and the flow transverse section varies from that in the pipeline. Where the flow is accelerated due to contraction, pressure falls and cavitation can occur. Its consequences are flow choking, erosion, malfunction or poor performance, limited life expectancy of the valve, wandering calibration of the attached instrumentation, piping fatigue, leakages, noise and vibrations [1].

In contrast to stop valves which operate either fully closed or opened and where cavitation can temporarily occur during position shifting, regulating valves are heavily jeopardized by cavitation if they do not suit the range of pressures and flow rates of a given application. This can be avoided if the valve characteristic for incipient cavitation is known. The proper characteristic of valve incipient cavitation is thus necessary for safe, low-cost and durable operation of the valve and the system where it is installed.

However, cavitation is strongly dependant on liquid quality, meaning the quantity of dissolved gas, microbubbles and impurities, which all act as nuclei for cavitation inception and promote an earlier onset of cavitation [2]. This should be also kept in mind when choosing the correct valve so that the designed operation limits are never exceeded.

The paper describes an experimental study of the cavitating flow through an axial valve. States of incipient cavitation were optically determined and analysed using visualization method. Simultaneously, pressure oscillations were measured with hydrophone, immersed in water downstream of the valve.

Conventionally, incipient cavitation is determined by the vigorous increase of noise level or vibrations [3–5], but these are only its consequences. Vibrations are conveniently measured with accelerometers mounted on valve body or piping. Still more, noise level can be significantly affected by other sources and measurements are sometimes done in industrial environment where total noise level is already high. In this manner, fast pressure transducers for pressure fluctuations are a better choice [6]. Similarly, visualization method enables fluid flow to be observed directly as it is, which means that we can also identify the precise location of cavitation and monitor its development [7]. Thereby the geometry of the valve can be redesigned to effectively modify the valve operating range without waiting for erosion damage to identify valve weak points. However, the visualization method used in our case should be distinguished from the visualization of flow patterns, with which valve performance can be also improved [8].

Experimental data were obtained for fully and half-open valve for five different operating pressures p_∞ from 75 to 175 kPa. For

* Corresponding author. Tel.: +386 1 4771 422; fax: +386 1 2518 567.
E-mail address: aljaz.osterman@fs.uni-lj.si (A. Osterman).

0894-1777/$ - see front matter © 2009 Elsevier Inc. All rights reserved.
doi:10.1016/j.expthermflusci.2008.12.008

Nomenclature

A	pixel brightness level (–)
C_D	drag coefficient (–)
D	diameter; characteristic (m)
$f_{S,\max,P,V}$	frequency; shedding, maximum in spectrum: of pressure oscillations, of visualization (Hz)
Δf	frequency step in spectrum (Hz)
F_D	drag force (N)
I	intensity (–)
i	column index (–)
j	row index (–)
L	cavity length (M)
n	picture index (–)
$p_{1,2,\infty,V}$	pressure; upstream, downstream, referential, vapour (Pa)
Δp	pressure difference (Pa)
$Q_{1,2,i,90\%,110\%}$	volume flow rate; 1st and 2nd valve opening, incipient, 90% and 110% of incipient cavitation ($m^3 s^{-1}$)
$Re = \frac{UD}{\nu}$	Reynolds number (–)
$St = \frac{f_S L}{U}$	Strouhal number (–)
T_∞	temperature; referential (K)
U	velocity; in pipeline, referential (ms^{-1})
z	cavitation index (–)
μ	image brightness level (–)
ν	kinematic viscosity ($m^2 s^{-1}$)
ρ_L	density; liquid ($kg\ m^{-3}$)
σ_i	cavitation number; incipient (–)

each, the flow at which incipient cavitation occurred was determined by observing the flow through the window in the valve body, waiting for the first bubbles to appear while simultaneously increasing the flow rate. Thus subject to personal perception, it was repeated many times with high repeatability. Also the sensitivity of the valve to cavitation was high (small changes in flow rate caused great changes of cavitation). In the next steps, the valve was subjected to a flow rate that was 1.1 and 0.9 of the flow rate of incipient cavitation Q_i, so that a comparison to non-cavitating and fully cavitating regime was made. In each operating point, which are all presented in Fig. 1, series of pressure oscillations from hydrophone and series of images taken by a camera were recorded on a computer.

2. Experimental set-up

A modified axial valve for pressure difference-based flow rate regulation was used. It was modified so that the closing element for flow rate regulation was moved manually. For visualization purposes a hole was made in the valve body and a transparent window from acrylic glass was inserted (Fig. 2). Furthermore all inner surfaces were painted black except for the observation window. The geometry of the channel was preserved. Regarding where cavitation is most likely to occur, the location for the observation window was chosen according to the smallest area of the channel transverse section and previous experiences.

The valve was mounted in a small cavitation test rig. The whole set-up is presented in Fig. 3.

The quantity of water in the loop was approximately 1 m^3. It was driven by a pump through a pipeline where the discussed axial valve was installed. Unprepared tap water was used for the experiments. Since the amount of dissolved and undissolved gasses can significantly influence the results, Van Slyke's method [9,10] was used to monitor water gas content before and after the experiment – it was held almost constant at 27 $mg_g/l_w \pm 5\%$ of the value.

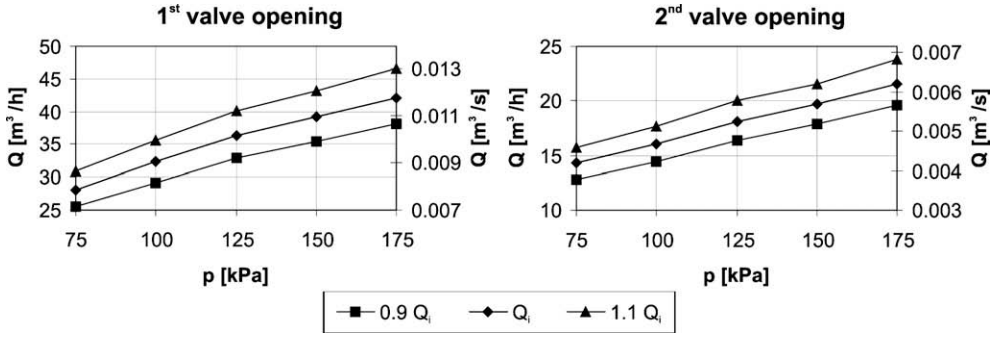

Fig. 1. Measured operating points (left-1: fully open, right-2: half-open).

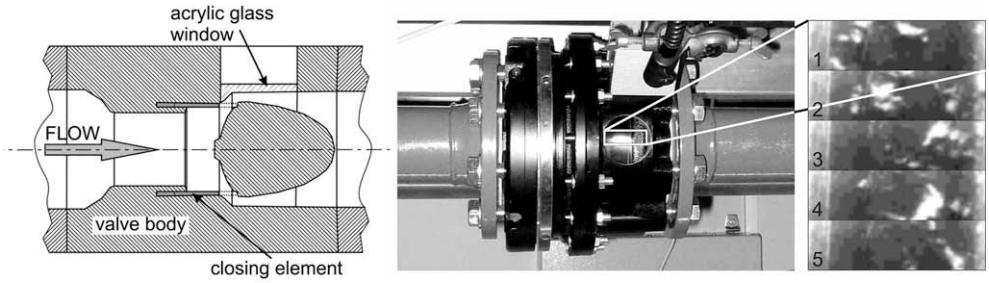

Fig. 2. Axial valve and simplified scheme of the valve longitudinal section.

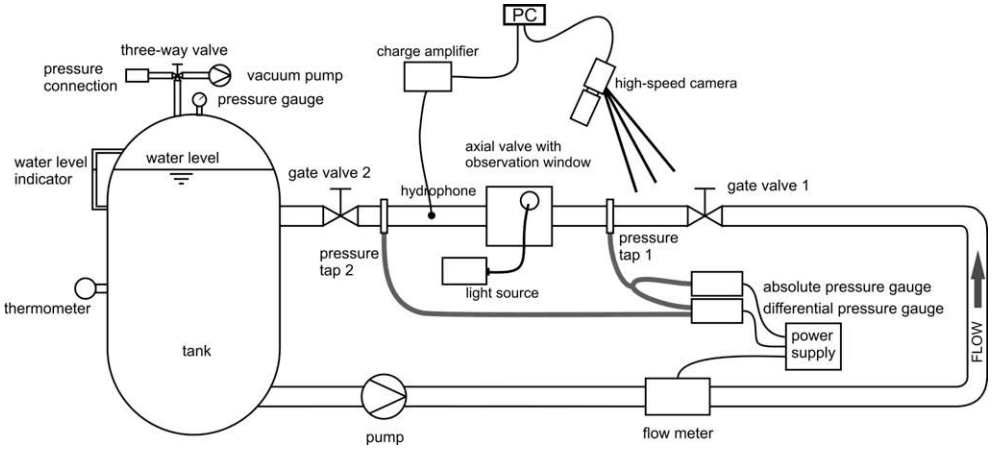

Fig. 3. Experimental set-up.

Operating pressure in the system was set by a vacuum pump or compressed air. Pressure was measured with an absolute and a differential pressure gauge (ABB 2600T Series, models 264 VS and DS, respectively), taken away circularly at four connections 8D upstream and downstream of the valve with reference point at valve axis. The uncertainty of the pressure measurement was ±0.075% of the value.

Volumetric flow rate was measured with an electromagnetic flow meter ABB COPA-XL DL43F DN 125/PN 16. The measurement uncertainty of the volumetric flow rate was up to ±1% of the value.

The experiment was performed with water temperature close to the ambient (T_∞ = 24 °C). It was measured with a Pt100 thermometer with uncertainty of ±0.5% in a range from 0 to 100 °C. The test rig was left to stabilize by running it 1 h previous to the beginning of the experiment, so water temperature was constant during the experiment.

Pressure oscillations were measured with a Bruel and Kjaer type 8103 hydrophone, connected to a B&K 2635 charge amplifier and then led as voltage signal to a PC. Hydrophone sensitivity was 0.103 pC/Pa ±2 dB, frequency range was from 2 Hz to 100 kHz, while acquisition frequency was set to 50 kHz and sample length was 5 s. The hydrophone was mounted elastically to the piping 1D downstream the valve and there was no cavitation on it. A position for hydrophone was chosen as close as possible to the valve. Because of its relatively small diameter (DN 65) and because of an estimation that a vapour volume fraction away from the valve cavitating zone was practically zero, it can be assumed that pressure oscillations reached the hydrophone undamped.

For visualization a CCD Dragonfly Express (Point Grey Research) digital camera was used with Edmund Optics Double Gauss 75 mm lenses. The signal was led directly to the PC via IEEE 1394 interface. The illumination was provided by a continuous light source VEGA VELUM 150 DR with an EKE 21V 150 W lamp. The light was transmitted via optical fibre to the observation window in the axial valve. Image size was 320 × 90 pixel which covered the area of 21 × 6 mm. Camera frame rate was at 500 Hz with exposure time of 10^{-4} s, series length was around 3 s. Lighting, short exposure time and good spatial resolution of the images assured that even the smallest details in the flow were seen, so we can assume that also for the first bubbles of incipient cavitation.

3. Measurements and data analysis

3.1. Operating conditions

For characterization of cavitation a cavitation number σ is used [2]:

$$\sigma = \frac{p_\infty - p_V(T_\infty)}{\frac{1}{2}\rho_L U^2}. \tag{1}$$

By knowing volume flow rate and pipeline diameter, referential velocity U in the pipeline is calculated from continuity equation.

For valves, a cavitation index is used instead of a cavitation number [3,4,8,11]:

$$z = \frac{\Delta p}{p_1 - p_V} = \frac{\Delta p}{p_\infty - p_V}. \tag{2}$$

In our case $p_1 = p_\infty$ and $\Delta p = p_1 - p_2$ (upstream pressure–downstream pressure). Considering the measurement uncertainties of pressure, velocity and temperature measurements, the cavitation number (Eq. (1)) or the cavitation index (Eq. (2)) could be determined within ±1.5% of the value.

Pressure difference Δp is connected to drag force F_D, which can be expressed for turbulent flow in the valve (Re > 10^4 at all points) as:

$$\Delta p \propto F_D = C_D \frac{\rho U^2}{2}. \tag{3}$$

C_D is drag coefficient, ρ is fluid density and U is referential velocity.

For better comparison with σ, an inverse cavitation index is defined (sometimes also named cavitation index [1,6]):

$$z^{-1} = \frac{p_\infty - p_V(T_\infty)}{\Delta p}. \tag{4}$$

For both it is true that the lower they are, the more extensive cavitation is. In Fig. 4, σ and z^{-1} are presented for all measured points (pressures 8D upstream and 8D downstream, system temperature and flow velocity at the valve inlet were used as reference values).

Cavitation is stronger for higher flow rates where σ and z^{-1} are lower. From the diagrams it can be also seen that the cavitation number for incipient cavitation does not change much while the inverse cavitation index is increasing with the operating pressure (particularly for the 1st valve opening). As pressure difference on a valve is proportional to drag, which is proportional to U^2 and the drag coefficient (Eq. (3)), a qualitative comparison between σ and z^{-1} gives that with the rising operating pressure the drag coefficient must be decreasing.

3.2. Computer aided visualization

For series of images, obtained by visualization method, settings for brightness and contrast were constant and equal for all points during the experiment.

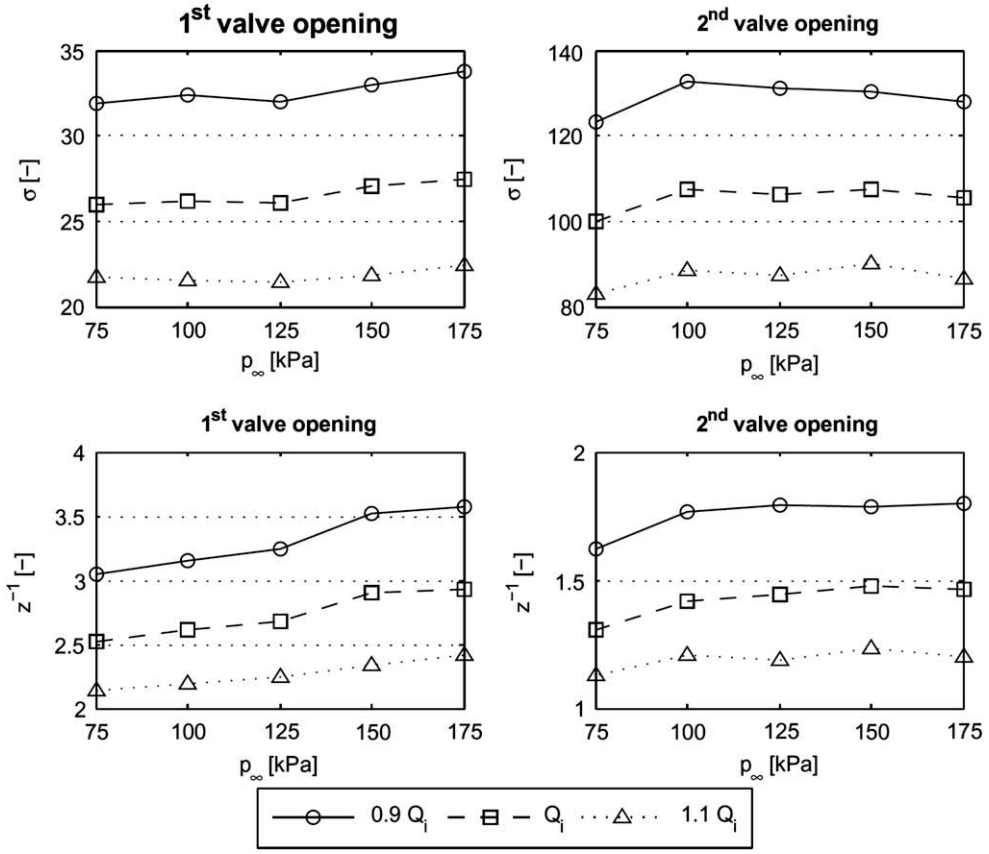

Fig. 4. Cavitation number and inverse cavitation index for measured operating points for both valve openings (left-1: fully open, right-2: half-open).

The camera was acquiring series of eight-bit greyscale images that were showing cavitation inside the valve. Although the exact relationship between the size of cavitation and image brightness is not known, certainly the void fraction and thus cavitation size are proportional to the measured pixel brightness. Image post-processing is based on the fact that image n with ij pixels can be presented as a matrix with ij elements. Eight-bit resolution gives 256 levels of grey level $A(i,j,n)$, which the matrix element can occupy (0 for black pixel and 255 for white pixel):

$$A(i,j,n) \in \{0,1,\ldots,255\}. \tag{5}$$

Each image is presented as a matrix:

$$\mathrm{Image}(n) = \begin{pmatrix} A(1,1,n) & \cdots & A(I,1,n) \\ A(1,2,n) & \cdots & A(I,2,n) \\ \vdots & \ddots & \vdots \\ A(1,J,n) & \cdots & A(I,J,n) \end{pmatrix}. \tag{6}$$

For the present evaluation the brightness of each image was calculated by averaging the brightness of the pixels in the image:

$$\mu(n) = \frac{1}{I \cdot J} \sum_{i=1}^{I} \sum_{j=1}^{J} A(i,j,n)$$

From brightness values μ(n) time series were formed for spectrum analysis. Time series were transformed using fast Fourier transformation (FFT) algorithm into discrete Fourier transform (DFT) so that frequency spectra were obtained. According to Nyquist's sampling theorem, the highest relevant frequency was 1/2 of the acquisition frequency.

Data analyses were done with Matlab.

4. Discussion of results

4.1. Hydrophone

FFT transformed pressure oscillations time series and frequency spectra were obtained. In Fig. 5, a hydrophone signal for incipient cavitation at p_1 = 125 kPa for the first valve opening (fully open) is presented. On the left side, a log–log scale is used in order to present the high frequency noise. On the right side, the same signal is presented with linear ordinate axis. According to the actual proportions of power spectral density (PSD) values, the interesting frequency range spans to no more than 200 Hz (although some references indicate that higher frequencies [6,12] are more interesting than lower [13]). For better comparison with the visualization data, further diagrams of frequency spectra are all presented in the range up to 250 Hz.

Furthermore, frequency spectra obtained from hydrophone signals for one operating pressure (in this case 125 kPa) are presented in Fig. 6. Firstly, an apparent change in PSD magnitude occurs when the valve is half closed. The incipient cavitation volume flow rate for the second opening is only half the previous. As presented in Fig. 4, the cavitation number also significantly alters. Next, the spectrum magnitude rises with the rising volume flow rate. This is expected because cavitation is also becoming larger.

4.2. Visualization

Frequency spectrum diagrams for visualization (for operating conditions appurtenant to Fig. 6) are presented in Fig. 7.

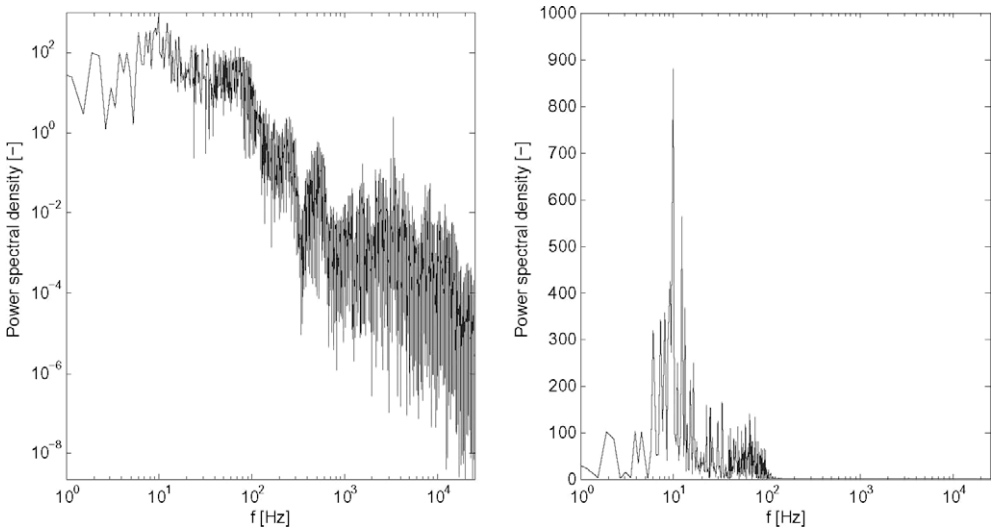

Fig. 5. Spectrum from hydrophone signal presented in log–log and log–linear scales.

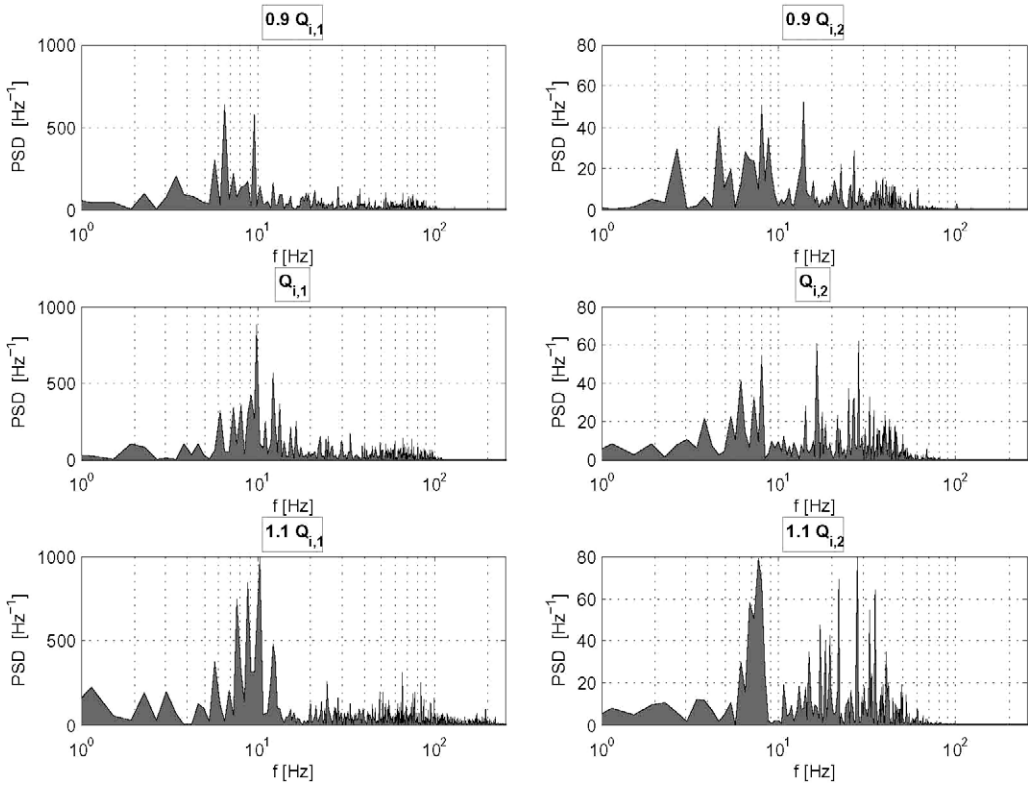

Fig. 6. Frequency spectra from hydrophone measurements at 125 kPa for both valve openings and 0.9, 1 and 1.1 of incipient cavitation volume flow rate Q_i (left-1: fully open, right-2: half-open).

Visualization spectra show great change in PSD magnitude between cavitating and non-cavitating conditions (1.1 and $0.9Q_i$), while the magnitude of incipient cavitation spectrum depends on how well it was optically determined in the first place. As the aforementioned intensity change between 1.1 and $0.9Q_i$ is several orders of magnitude, this practically means great sensitivity to cavitation. Also in contrast to pressure oscillations spectra (Figs. 5 and 6), there are no distinct frequency peaks.

4.3. Comparison of the methods

As mentioned before, hydrophone readings of pressure oscillations are apart from cavitation size also dependent on operating pressure and valve opening. Fig. 8 shows, for the case of incipient cavitation, how frequency peaks are shifted towards higher frequencies, as well as the fact that the magnitude of the signal rises with increased operating pressure. Additionally, the range with the

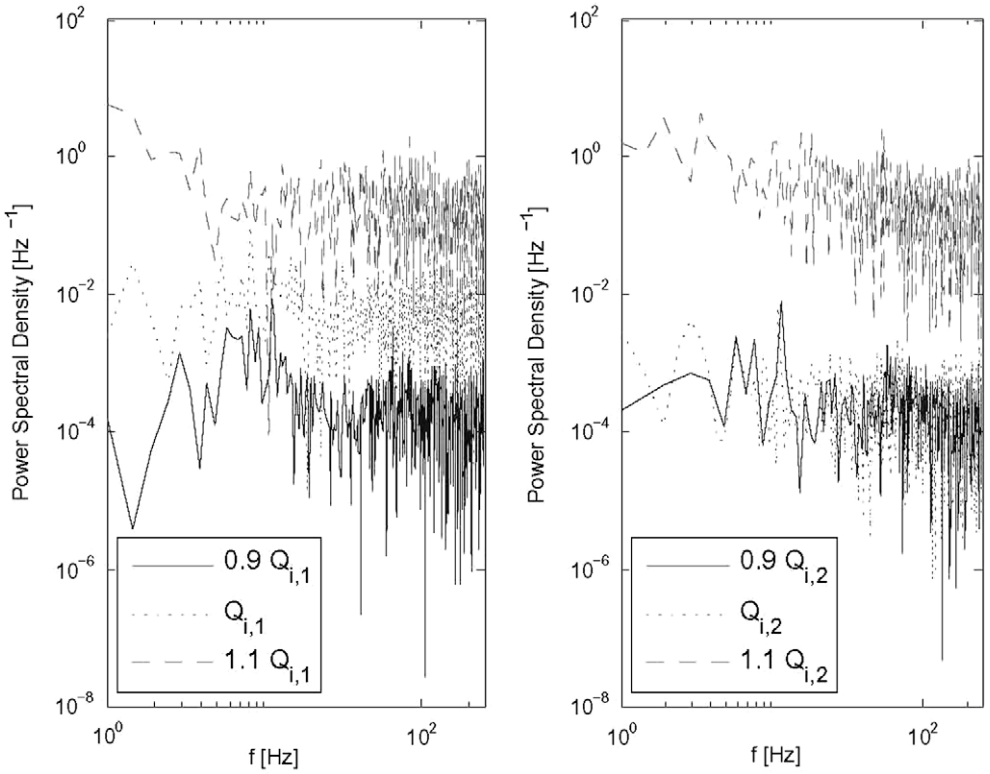

Fig. 7. Frequency spectra from visualization at 125 kPa for both valve openings and 0.9, 1 and 1.1 of incipient cavitation volume flow rate Q_i (left-1: fully open, right-2: half-open).

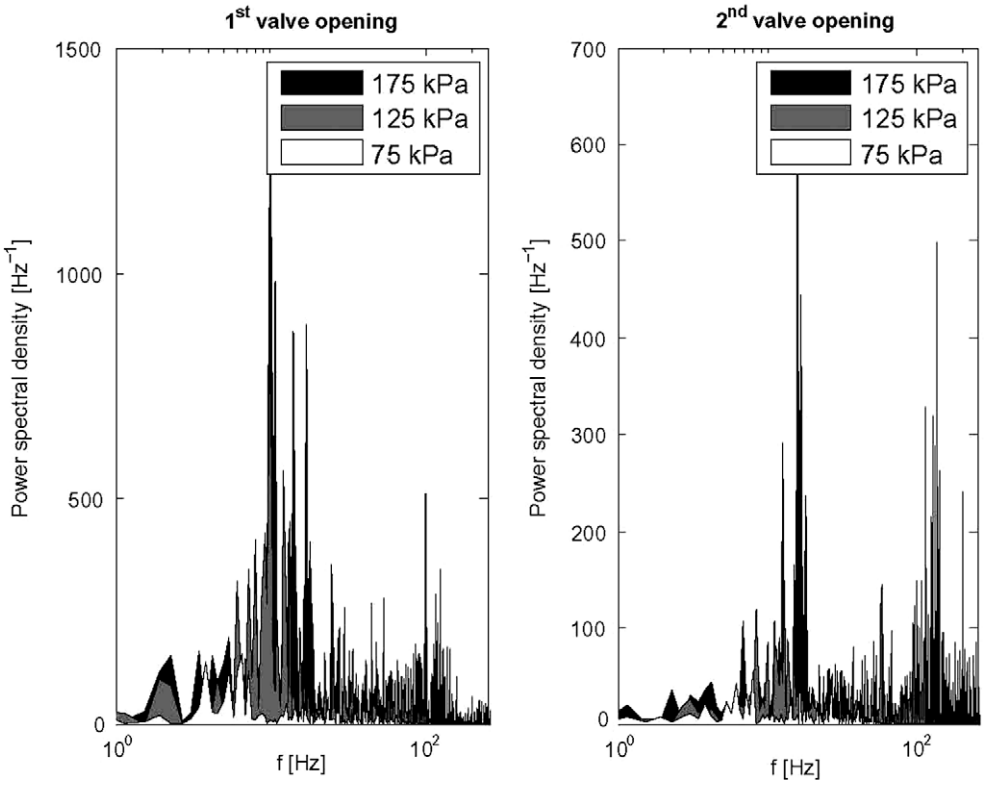

Fig. 8. Spectra based on hydrophone data for incipient cavitation at different operating pressures (left-1: fully open, right-2: half-open).

largest PSD contribution in a spectrum is also shifted towards higher frequencies. Most probably the frequencies are augmented because at higher pressures velocities are increased to achieve incipient cavitation, so if Strouhal number that describes the

frequency of cavitation shedding f_S is to be kept constant [14], the frequency of cloud shedding must increase for the same size of cavitation L.

Strouhal number is [14]:

$$St = \frac{f_S L}{U}. \tag{7}$$

Although there are signal differences for the same type or size of cavitation (Fig. 8), if stuck to the same operating pressure and valve opening, hydrophone signal exhibits good correlation to the cavitation extent. Fig. 9 presents frequency spectra from hydrophone data for both valve openings for different operating pressures.

The first row presents states with no cavitation, the second presents incipient cavitation and in the third row shows results for the developed cavitation. If the signal at the same operating pressure is observed, a significant increase of PSD is noticeable as the cavitation grows. Although the increase and the decrease of the volume flow rate of incipient cavitation are the same (10%), the signal changes more from Q_i to $1.1Q_i$ than from $0.9Q_i$ to Q_i, which is expected because incipient cavitation has little influence on the flow.

Comparison between the results of spectrum analysis of hydrophone and visualization data, makes it obvious that the former does not show so great differences between signals recorded at different operating pressures (Fig. 10). The most striking feature of the diagrams in Fig. 10 is how the PSD values increase for two or more orders of magnitude when we move from the state without cavitation to the state of developed cavitation. This implies to the great sensitivity of the method.

For better comparison, PSD from frequency spectra from both visualization and hydrophone data for all points were integrated to obtain signal intensity:

$$I = \sum_{0}^{f_{max}} \mathrm{PSD} \cdot \Delta f, \tag{8}$$

Intensity is calculated for the whole frequency range. Maximum frequency for pressure oscillations is $f_{max,P}$ = 25 kHz and for visualization $f_{max,V}$ = 250 Hz. Δf is frequency step defined by the FFT. Normalized intensity values are presented in Fig. 11.

For hydrophone data, increase in signal intensity is mainly due to higher operating pressure, because at higher pressures cavitation as well as turbulent pressure fluctuations are more powerful. On the contrary, visualization shows that for a certain type of flow (cavitating or non-cavitating) signal intensity fits a certain range regardless of the operating pressure. A favourable fact is also that the intensity values vary so much that the logarithmic scale was used, what again points to the great sensitivity of the visualization method (compared to the hydrophone measurements).

However, if visualization results for incipient and non-cavitating conditions are compared for both valve openings, they are quite different. It was estimated that in the first case incipient cavitation was slightly more extensive than in the second, where it was set a bit closer to a non-cavitating state. This is due to subjective determination of the operating point for incipient cavitation. Another possible reason would be a coincidental nature of cavitation, where longer recorded sequences might give better results.

To further investigate the accuracy of visualization with respect to the hydrophone measurements for determination of the incipient cavitation, the signal intensity was plotted against the flow rate (as proposed by Tullis [5]) as shown in Fig. 12 for both methods. Only a case of operating pressure of 125 kPa is presented (for both valve openings) – the results for other cases are comparable. It is obvious that a change in a gradient is considerably higher in a case of visualization then in a case of hydrophone measurements.

By using visualization technique the conditions for the first occurrence of cavitation bubbles can be relatively easily and accurately predicted. As the cavitation first appears, its extent and consequently signal intensity grow linearly as the flow rate is increased, hence one only has to measure the intensity of the signal

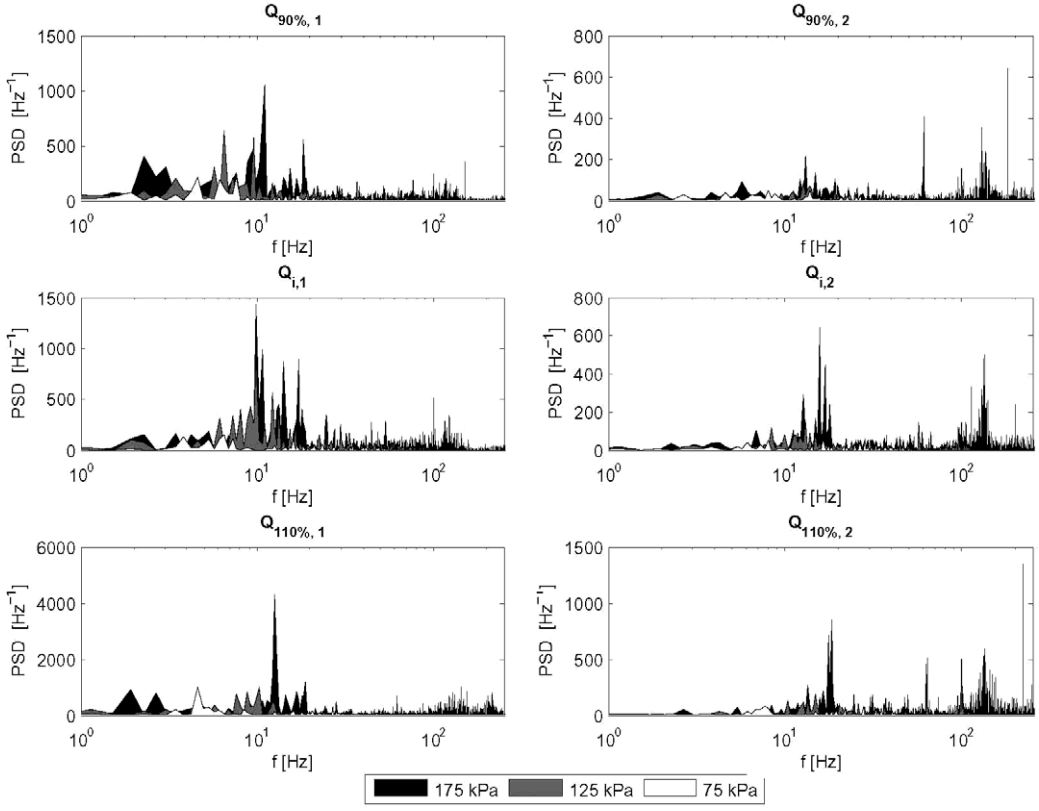

Fig. 9. Frequency spectra from hydrophone data for different operating pressures and volume flow rates (left-1: fully open, right-2: half-open).

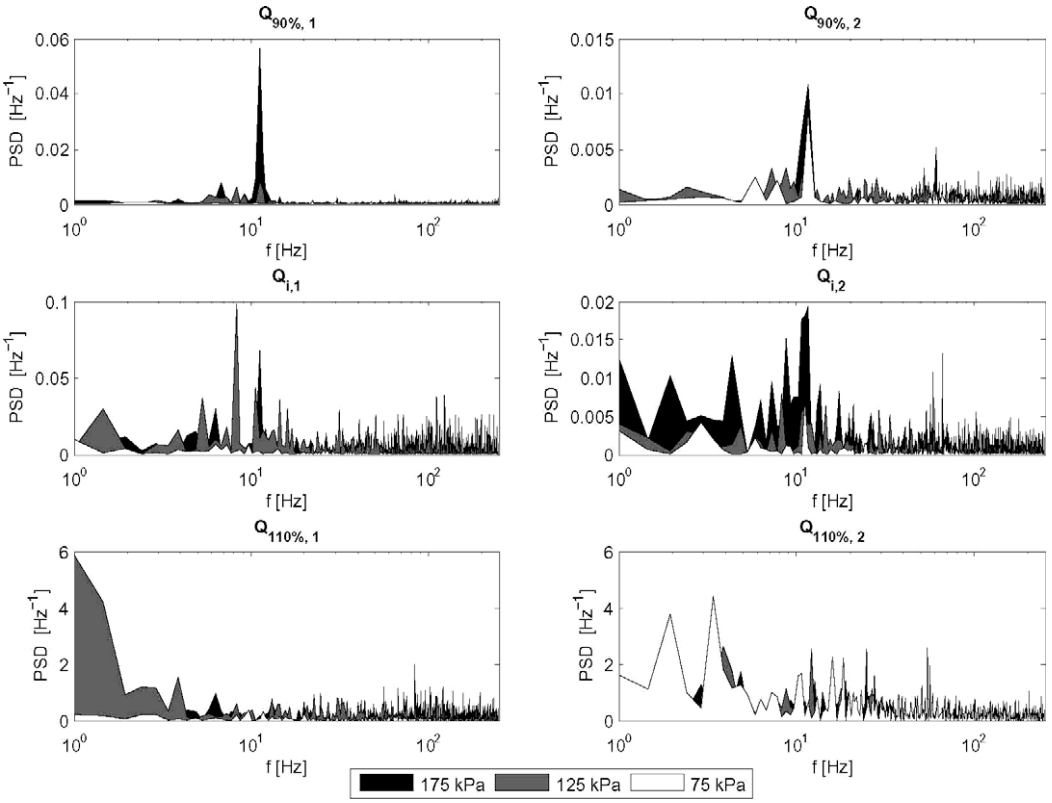

Fig. 10. Spectra from visualization data for different operating pressures and volume flow rates (left-1: fully open, right-2: half-open).

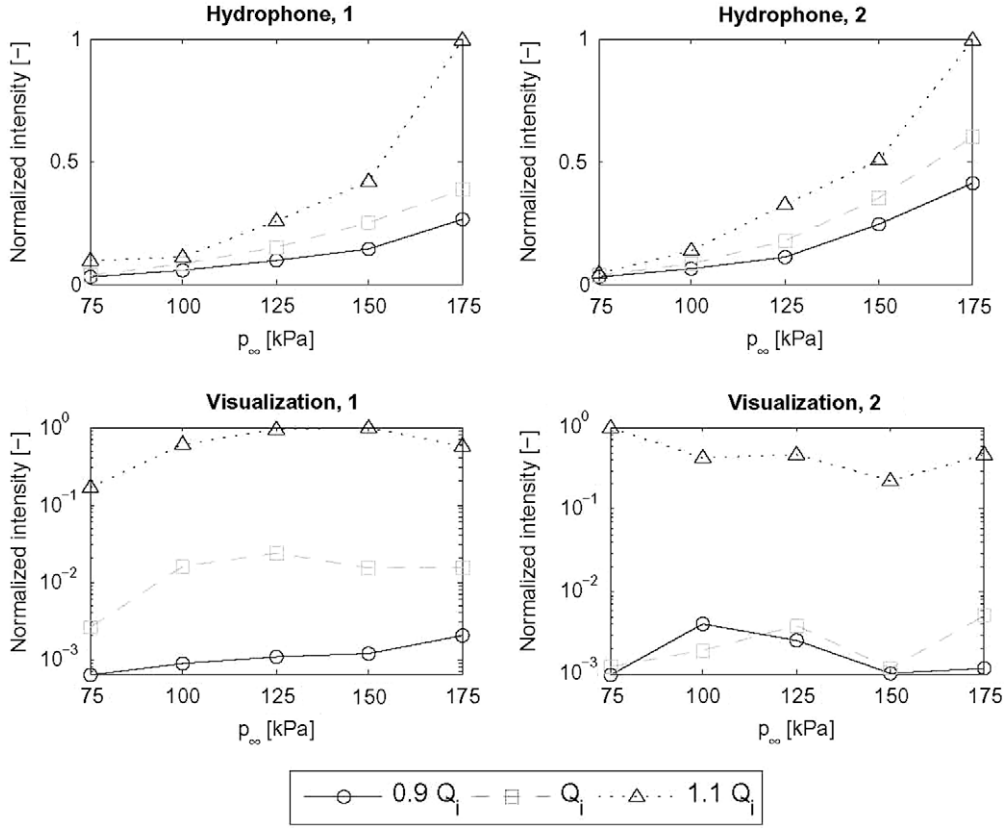

Fig. 11. Normalized intensity for hydrophone and visualization signals for both valve openings (left-1: fully open, right-2: half-open).

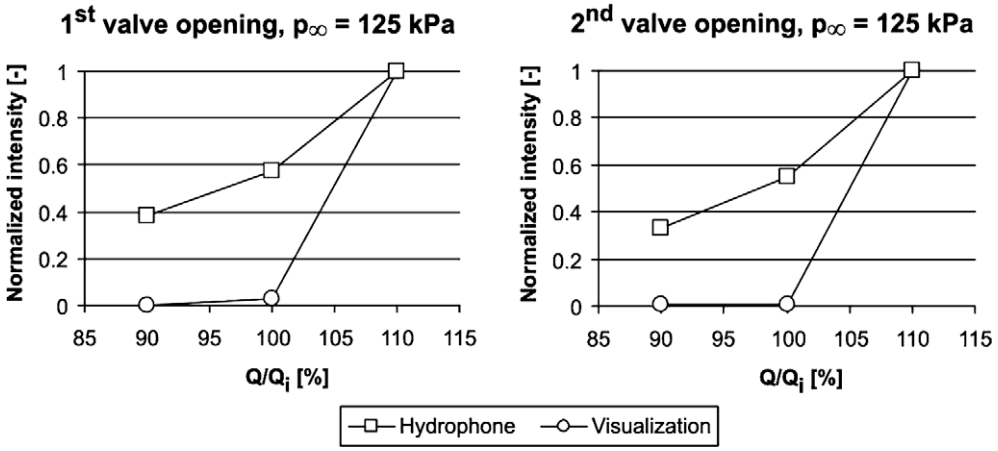

Fig. 12. Normalized intensity for hydrophone and visualization signals as a function of flow rate for both valve openings (left-1: fully open, right-2: half-open).

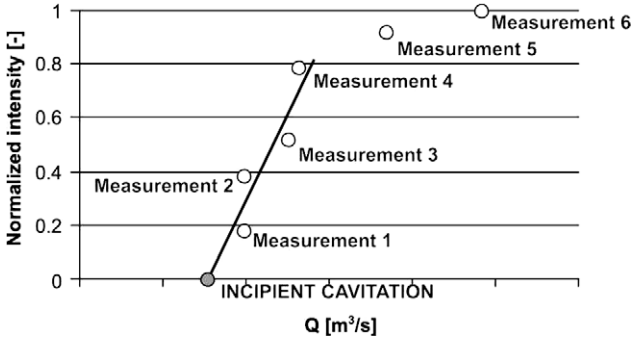

Fig. 13. Determination of incipient cavitation by visualization method.

for at least two operating points of developed cavitation (more measurements of course increase the accuracy of the method). Extrapolation of the line to the signal value of 0 reveals the conditions of incipient cavitation. It must be emphasized that the points at which the signal intensity is measured should lie as close as possible to the incipient cavitation and should in no case represent the condition of choked flow or supercavitation – the linear relationship is not valid in such case and the accuracy of the method deteriorates significantly – again this problem can be avoided by performing several measurements instead of only two.

Fig. 13 schematically shows determination of the incipient cavitation conditions by visualization method. An example in Fig. 13 shows how six measurements are performed to increase accuracy. Measurements 5 and 6 lie at higher flow rates and are close to choking flow – the linear relationship is not valid so they are not included in the evaluation later. Measurements 1, 2, 3 and 4 show linear relationship. Extrapolating a line obtained with linear regression to a value of intensity 0, we get the conditions of the incipient cavitation (marked by the darker circle in the diagram).

It is considerably harder or even impossible to use hydrophone measurements in the same manner. There is always some background noise present (the signal intensity does not fall to 0 when cavitation is not present) and there are additional parameters that one should consider – for example a system pressure. Furthermore, as already mentioned, change in gradient is not as significant as in the case of visualization, and it is therefore harder to determine.

5. Conclusions

For the evaluation of incipient cavitation in an axial valve two methods were compared: the measurement of pressure oscillations downstream the valve with a hydrophone and the visualization of the flow in the valve. This was done at different operating pressures and incipient cavitation was also compared to developed cavitation and non-cavitating state.

First, spectrum analysis was done. It showed no prominent peaks that would be useful for incipient cavitation estimation. Hydrophone analysis also showed great differences between signals describing the same flow conditions if operating pressure was changed.

Secondly, signal intensities were calculated from frequency spectra for all points for both methods. This confirmed that the hydrophone signal depends more on operating pressure than on cavitation. When defining incipient cavitation, the reference signal or final intensity value must therefore be set separately for each operating pressure. On the contrary, for visualization, signal intensity does not depend on operating pressure and favourably changes for several orders of magnitude, when flow goes from non-cavitating to fully cavitating. This means that the visualization method is more general and shows greater sensitivity.

It was shown that it is relatively simple to predict the operating conditions at which cavitation first appears when visualization method is employed, although it used information of a much lower frequency content than hydrophone measurements. In principle measurements at only two carefully selected operation points have to be performed (more measurements, of course, contribute to a more accurate result). On the other hand this could not be done by hydrophone measurements due to its dependency on several additional parameters such as system pressure.

Modification of the existing valve is a major drawback of the visualization method. The method is thus more applicable to cases where integrated parts are already transparent or can be easily replaced by such. When applied, the benefits of cavitation visualization, apart from mere determination of the operating range, outweigh additional work and costs for modification and because of that we can conclude that visualization method is especially suitable for valve design and testing.

References

[1] P.L. Skousen, Valve Handbook, second ed., McGraw-Hill, 2004.
[2] C.E. Brennen, Cavitation and Bubble Dynamics, Oxford University Press, 1995.
[3] AWWA Manual M49, Butterfly Valves, Torque, Head loss, and Cavitation Analysis, 2001.
[4] A.G. Samson, Technical Information: Cavitation in Control Valves. <www.samson.de>.
[5] J.P. Tullis, Hydraulics of Pipelines: Pumps, Valves, Cavitation Transients, John Wiley and Sons Inc., 1989.
[6] C.S. Martin, H. Medlarz, D.C. Wiggert, C. Brennen, Cavitation inception in spool valves, Journal of Fluids Engineering 103 (1981) 564–576.

[7] B. Širok, B. Blagojević, T. Bajcar, F. Trenc, Simultaneous study of pressure pulsation and structural fluctuations of a cavitated vortex core in the draft tube of a Francis turbine, Journal of Hydraulic Research 41 (5) (2003) 541–548.
[8] M.-J. Chern, C.-C. Wang, C.-H. Ma, Performance test and flow visualization of ball valve, Experimental Thermal and Fluid Science 31 (2007) 505–512.
[9] R. Streidinger, Ein Beitrag zur Bedeutung der Wasserqualität und von Massstabsgesetzen in Kreiselpumpen bei beginnenden Kavitation, PhD Thesis, TU Darmstadt, Darmstadt, 2002.
[10] F. Brand, Ein physikalisches Verfahren zur Bestimmung von gelösten und ungelösten Gasen in Wasser, Voith Forschung und Konstruktion, vol. 27, 1981.
[11] D. Đonlagić, B. Tovornik, Regulating valves, Fakulteta za elektrotehniko, računalništvo in informatiko, 1997 (Krmilni ventili, in Slovenian language).
[12] T. Koivula, On cavitation in fluid power, in: Proceedings of the 1st FPNI-PhD Symposium, 2000, pp. 371–382.
[13] H. Hassis, Noise caused by cavitating butterfly and monovar valves, Journal of Sound and Vibration 225 (3) (1999) 515–526.
[14] J.-P. Franc, J.-M. Michel, Fundamentals of Cavitation, Kluwer Academic Publishers, 2004.